Appl. Phys. A 79, 489–497 (2004)
DOI: 10.1007/s00339-004-2566-5

Applied Physics A
Materials Science & Processing

Invited paper

O. CONDE[1,✉]
A.J. SILVESTRE[2]

Laser-assisted deposition of thin films from photoexcited vapour phases

[1] Departamento de Física, Faculdade de Ciências da Universidade de Lisboa, Campo Grande, Ed. C8, 1749-016 Lisboa, Portugal
[2] Instituto Superior de Engenharia de Lisboa, R. Conselheiro Emídio Navarro 1, 1949-014 Lisboa, Portugal

Received: 29 December 2003/Accepted: 8 January 2004
Published online: 10 March 2004 •

ABSTRACT Laser-assisted chemical vapour deposition (LCVD) has been extensively studied in the last two decades. A vast range of applications encompass various areas such as microelectronics, micromechanics, microelectromechanics and integrated optics, and a variety of metals, semiconductors and insulators have been grown by LCVD. In this article, we review briefly the LCVD process and present two case studies of thin film deposition related to laser thermal excitation (e.g., boron carbide) and non-thermal excitation (e.g., CrO_2) of the gas phase.

PACS 81.15.Fg; 81.15.Kk

1 Introduction

Chemical vapour deposition (CVD) has been one of the most widespread technologies for fabricating thin films and coatings. It has long been used in the manufacture of very different types of films for a variety of applications, either as protective or functional coatings [1]. In a conventional (thermal) CVD process, a solid product is formed as the result of a chemical reaction occurring in a gas or vapour phase near or on the surface of a substrate. The reaction is thermally activated, i.e., the substrate is directly and uniformly heated, and an extended uniform film of the deposited material is obtained onto the substrate. By comparing CVD with physical vapour deposition (PVD) processes, CVD has a higher throwing power. In fact, it is not restricted to a line of sight deposition, allowing to coat deep recesses, holes and other three-dimensional features with different shapes and sizes [1].

However, the increasing complexity and miniaturisation of systems needed in such areas as microelectronics, micromechanics, microelectromechanics and integrated optics, require controlled area coating techniques which avoid excessive application of chemicals. This is achieved in CVD, and other large area deposition techniques, by employing a sequential application of mechanical masking and/or lithographic methods. Nevertheless, these procedures are time-consuming and often difficult to apply, especially if the substrate is non-planar. Further, for many of the chemical reactions used in the deposition of materials with interesting properties, the chemical reaction threshold temperatures are relatively high, usually above 1000 °C, which limits the ability to coat heat-sensitive substrates [2].

Therefore, whenever selective area growth is needed and/or heat-sensitive substrates are employed, the use of a laser beam to induce CVD (LCVD) is advantageous, overcoming the main drawbacks of CVD. For instance, LCVD offers spatial resolution of the deposited material, limited distortion of the substrate avoiding deleterious effect on bulk material properties, high purity films due to smaller heat affected zone and greater control of the grain size due to rapid non-equilibrium heating and cooling rates [3], ease of processing at 3D [4–6] and deposition rate enhancement [7].

LCVD was extensively investigated in the last two decades and a wide variety of metals, semiconductors and insulators have been deposited, mainly for microelectronic applications [7–11]. However, the use of LCVD as a deposition method is beyond the microelectronic field and may be successfully employed to deposit a vast diversity of materials useful in other technological branches. It is our purpose in this article to discuss the syntheses of two ceramic compounds, boron carbide (B_4C) and chromium dioxide (CrO_2), by laser-induced CVD using infrared and ultraviolet lasers respectively. These materials find quite different applications, B_4C being a wear-resistant superhard compound and CrO_2 a half-metallic material with special interest in the new and promising field of spin-electronics.

2 Laser-assisted chemical vapour deposition

Laser-assisted chemical vapour deposition can be based on two different mechanisms. Depending on the wavelength of laser radiation and on the precursor compounds and substrate material used, LCVD is governed by chemical reactions that are initiated by pyrolysis (photothermal or pyrolytic LCVD) or by photolysis (photochemical or photolytic LCVD). In many systems both pyrolytic and photolytic mechanisms contribute simultaneously to the reaction, although one of them may dominate the deposition process.

✉ Fax.: +351-21/7500-977, E-mail: oconde@fc.ul.pt

2.1 *Pyrolytic LCVD*

In pyrolytic LCVD the vapour phase is transparent to the laser radiation. The laser beam impinges on the substrate at perpendicular incidence and the chemical reaction is thermally driven through localised heating of the substrate surface by the laser radiation. With a stationary laser beam three-dimensional material structures can be grown. By moving the substrate relative to the laser beam, single-step deposited patterns may be generated. For example, in the case of a single translation, a stripe is drawn whose width and height depend on a large number of parameters including the optical and thermal properties of the substrate and film materials, the energy distribution profile of the beam, the laser power density, the scanning velocity, the chemical reaction threshold temperature and the reaction kinetics.

The microscopic mechanism for deposition is expected to be essentially the same as in thermal CVD, namely the thermal activation of the chemical reaction. As a consequence, all reactions observed in large area deposition can, in principle, be used in pyrolytic LCVD. Nevertheless, a number of fundamental new kinetic aspects arise in laser thermal deposition owing to the 3D character of the diffusion of the chemical species into the microreaction zone generated by the localised heat source. A major consequence of this is the observed strong enhancement of the deposition rate easing the growth of 3D microstructures [4].

Pyrolytic LCVD was first carried out by Lydtin [12], in 1972, related to carbon deposition on aluminium substrates, using an IR laser. Since that time almost all commercially available lasers have been utilised as radiation sources. When high spatial resolution is required, in particular submicron size patterns for microelectronic devices, argon and krypton ion lasers are preferred. Otherwise, Nd : YAG, Nd : glass and CO_2 lasers may be also employed – most gases do not absorb either visible or infrared wavelengths.

Photothermal LCVD can be also accomplished by vibrational excitation with IR laser light. By using an appropriate combination of the type of laser and the gas phase – chemical precursor and/or photosensitizer – some species can be excited vibrationally which leads to the heating up of the entire gas phase throughout collisional and vibrational relaxation processes. A CO_2 laser and BCl_3, SiH_4 or NH_3 are examples of such a combined system. In fact, these compounds present vibrational infrared-active modes within the CO_2 laser emission range [13–16].

2.2 *Photolytic LCVD*

Photo-induced CVD has attracted much attention as a low temperature technique for growing thin films. Both lamps and lasers have been used as photon sources. Because laser beams provide a much higher power density, growth rates can be increased by a factor of 10^2 compared to those obtained by employing conventional light sources [17]. Photolytic LCVD is thus a powerful technique for the growth of extended coatings on temperature sensitive materials.

In photolytic LCVD, film deposition occurs by direct bond breaking of precursor molecules due to resonant absorption of the laser radiation. The laser and precursor for photolytic LCVD are so chosen that the precursor molecules have a large absorption cross-section for the laser radiation and the chemical bond energy of the precursors is less than or equal to the energy of a single photon of the laser beam. Because most molecular bond energies are of several electron-volt [18], visible or UV laser light are generally required for dissociative-electronic excitation (Table 1).

Laser type	Spectrum region	λ (nm)	$\tilde{\nu}$ (cm^{-1})	E (eV)
CO_2	IR	10600	943.4	0.1
Nd : YAG	IR	1060	9434.0	1.2
Nd : Glass	IR	1060	9434.0	1.2
Cu vapour	VIS	511	19569.5	2.4
Ar^+	VIS	514.5	19436.4	2.4
Ar^+	VIS	488	20491.8	2.5
Kr^+	VIS	357.1	28082.0	3.5
Nitrogen	Near UV	337	29673.6	3.7
XeCl	UV	308	32467.5	4.0
KrF	UV	248	40322.6	5.0
KrCl	UV	222	45045.1	5.6
ArF	UV	193	51813.5	6.4

TABLE 1 Representative laser lines of several available commercial lasers

The usual experimental set-up for photolytic laser deposition is based on the parallel configuration, i.e., the laser beam passes parallel to the substrate surface at a certain distance, and the chemical reaction starts after the laser photons have been absorbed by the reactive gas phase. Therefore, this geometry allows an independent control of the substrate temperature during the deposition process. However, the perpendicular geometry can be also successfully used combining both photolytic and pyrolytic processes.

3 Laser-assisted deposition of boron carbide films

3.1 *Material properties and applications*

Hard coatings are primarily used to protect surfaces from abrasive wear. The importance of hard wear protective coatings in machining applications was recently illustrated by Veprek [19] who showed that more than 40% of all cutting tools are coated with wear resistant materials. Moreover, the availability of wear resistant superhard coatings for high speed dry machining would allow industries to increase the productivity of expensive automated machines and to save on the high costs presently needed for environmentally hazardous coolants [19].

Rhombohedral boron carbide, often denoted r-B_4C, is an intrinsic superhard material along with diamond and cubic boron nitride. It is the most stable compound in the boron-carbon system and exists as a single-phase material over a wide range of solubility, generally accepted from about 9 to 20 at % C. Its very high hardness (~ 40 GPa at room temperature) and abrasive resistivity, only inferior to diamond and cubic-BN, high melting point and modulus of elasticity, low specific weight, exceptional stability towards the effects of various acids and bases, etc. determine large possibilities for application of boron carbide in various branches of modern industry. Furthermore, above 1100 °C and in a nonoxidizing atmosphere, B_4C is the hardest compound known up to now [20], since diamond and cubic boron nitride tend to weaken at high temperature due to the transformation from the sp^3 cubic structure into the sp^2 hexagonal structure.

Besides mechanical applications, boron carbide is a ceramic material with potential applications in a wide variety of other fields [21]. For instance, given its high-temperature stability, large Seebeck coefficient and low thermal conductivity, potential use as high-temperature thermoelectric material for energy converters can be envisaged [21–23]. Furthermore, r-B_4C has found application as a neutron absorbent material in the nuclear industry [24] due to its high neutron capture cross-section through the reaction $^{10}B(n, \alpha)^7Li$.

The convergence of all these properties in one unique material reflects the complex structure of boron carbide, for which some uncertainty still persists [21, 25, 26]. The most accepted model for the rhombohedral structure of boron carbide considers $B_{11}C$ icosahedra clusters directly linked by covalent bonds and indirectly linked by a C–B–C chain along the main diagonal of the rhombohedron [21, 25–29]. Based on this model, boron carbide has a $B_{12}C_3$ stoichiometry with 20 at % C. The wide range for carbon content allowed by the phase diagram is made possible by the substitution of boron and carbon atoms for one another within both $B_{11}C$ icosahedra and C–B–C chains.

Deposition of boron carbide by CVD has been achieved on many substrates by using a mixture of methane and boron trichloride [30–34] or boron tetrachloride [35], at temperatures between 1000 and 1600 °C. Besides CVD techniques, r.f. sputtering [36], dc magnetron sputtering [37] and laser ablation [38] have also been used to prepare boron carbide thin films.

The deposition of boron carbide by Laser-CVD was shown from a dynamic reactive atmosphere of BCl_3, CH_4 or C_2H_4, and H_2 in conjunction with a continuous wave CO_2 laser [39–44]. As will be discussed the change from CH_4 to C_2H_4 is advantageous for the deposition process because it leads to improved film thickness control and higher deposition rates over lower carbon content in the gas phase.

3.2 *Experimental*

Figure 1 shows schematically a typical set-up for a laser CVD experiment. It consists mainly of a laser, a stainless steel vacuum chamber, a high vacuum pumping system and a gas system which delivers the reactants into the reactor.

The boron carbide films were deposited on silica substrates by using a dynamic reactive gas mixture of BCl_3 as a boron precursor, CH_4 or C_2H_4 as a carbon precursor, H_2 as a reducing agent and Ar as a buffer gas. The beam of a cw CO_2 laser, operating in TEM_{00} mode at a wavelength centred at 10.6 μm, reaches the substrate at perpendicular incidence and no focal lens was used since silica absorbs ~ 84% of the laser radiation. The substrates were kept stationary under the laser beam; therefore, the experimental variables to be controlled are the laser output power, interaction time, total pressure and partial flow rate of each gas (Φ_i). The relative amount of carbon and boron precursors in the reactive gas phase is characterised by the following parameter

$$\varphi = \frac{n\,\Phi_{HC}}{n\,\Phi_{HC} + \Phi_{BCl_3}} \qquad (1)$$

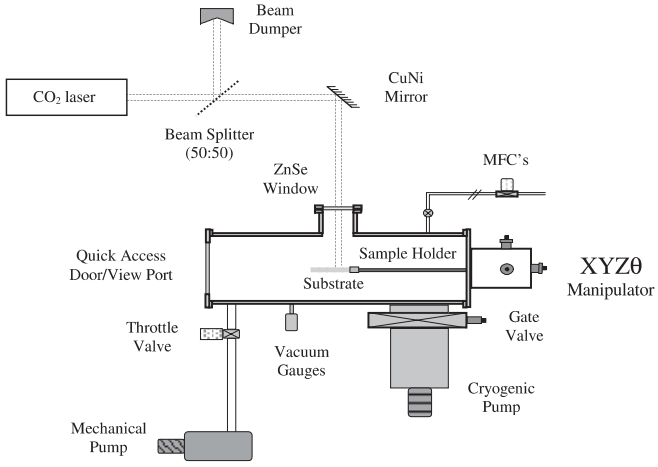

FIGURE 1 Experimental set-up for LCVD of r-B_4C films

where $n = 1$ for $HC = CH_4$ and $n = 2$ for $HC = C_2H_4$. As will be seen, φ is a key parameter influencing critically the chemical composition of the films.

3.3 *LCVD versus CVD: a thermodynamic comparison*

Figure 2 compares the carbon content of boron carbide films grown by thermal CVD and CO_2 laser CVD from similar gas mixtures consisting of BCl_3, CH_4 and H_2. The films deposited by CVD were synthesised at temperatures in the range 1200 K to 1500 K [30, 34] while for LCVD the processing temperatures were estimated at 800 K to 1100 K [40]. In the figure, the region between the horizontal dashed lines, at 9 and 20% carbon content levels, represents that one where r-B_4C may be formed.

As can be seen, deposition of r-B_4C by CVD is only achieved at high φ values, i.e., above 0.35 in the work of Jans-

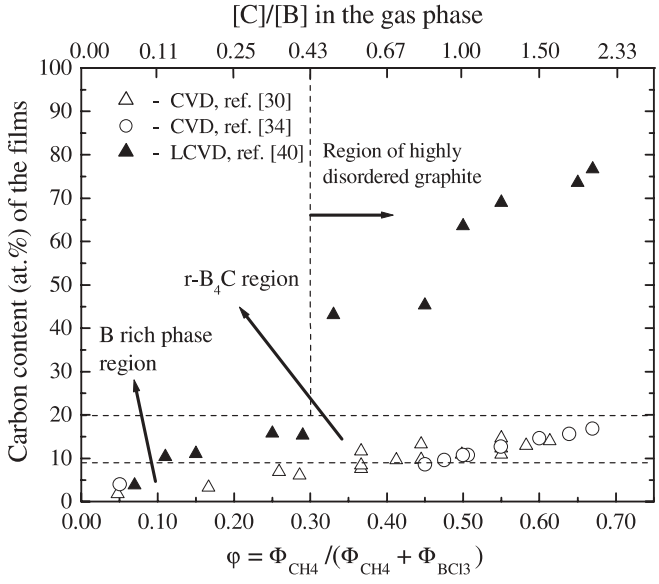

FIGURE 2 Carbon content vs. φ parameter for films deposited by CVD and LCVD using BCl_3, CH_4 and H_2. The r-B_4C region is bound by the *horizontal dashed lines* while the *vertical dashed line* indicates the region where disordered graphite is deposited in LCVD

son et al. [30] and 0.45 in that of Rey et al. [34], the latter value meaning close concentrations of carbon and boron in the gas phase. For lower carbon contents in the reactive atmosphere a boron-rich phase with different crystallographic structure ($B_{25}C$ or B_8C) is always deposited. Furthermore, in both CVD investigations, free carbon deposition was never observed, even when φ values as high as 0.67 were used.

By contrast, the stoichiometry of the LCVD films is much more sensitive to variations of φ. The [C]/[B] ratio in the coatings strongly increases with the [C]/[B] ratio in the reactive atmosphere. For values of φ up to 0.11 the LCVD films present a $B_{25}C$ stoichiometry while for $0.11 \leq \varphi \leq 0.29$ the carbon content is in the r-B_4C carbon allowed range. For higher carbon concentration, $\varphi > 0.29$, the measured carbon concentration in the films greatly exceeds the boron carbide content range, occurring in the deposition of disordered graphite with incorporation of boron atoms and no boron carbide formation [39] being observed.

These results show that a large difference between CVD and LCVD experimental deposition diagrams exists. Due to the main characteristics of laser radiation, it is often assumed that laser materials' processing may lead to non-equilibrium microstructures and compositions [3]. Therefore, the comparison with equilibrium thermodynamic predictions may help to clarify the nature of the discrepancies between CVD and LCVD diagrams. Thermodynamic calculations were performed using the computer program Solgasmix [45] in which a free-energy minimising technique is used to determine the equilibrium composition of a reactive chemical system. BCl_3 (g), CH_4 (g), H_2 (g) and Ar (g) were considered as reactants, according to the experimental work. B (rhombohedric), C (graphite) and r-B_4C were the only solid products to be found because the thermodynamic database for boron carbides only refers to r-B_4C. Data for other boron carbide stoichiometries were unavailable [40]. The main gaseous products were Ar (g) and HCl (g). Calculations were carried out for φ values between 0 and 1 and for temperatures in the range 300–1600 K. In each calculation the total pressure was kept at the experimental value of 1.33×10^4 Pa and the number of moles of each reactant was chosen in order to simulate the corresponding experimental partial pressure. Figure 3 summarises the results obtained, showing the equilibrium diagram where the distribution of solid phases is plotted as a function of temperature and gas phase composition.

The main results from thermodynamic calculations can be summarised as follows: i) pure r-B_4C is primarily formed at lower temperatures, the threshold temperature being nearly independent of the gas phase composition; ii) at higher temperatures, rhombohedric boron is formed along with r-B_4C for $\varphi < 0.1$ while for $\varphi \geq 0.2$ both r-B_4C and graphite are formed. The threshold temperature for graphite formation decreases as φ increases. As a consequence, the temperature range where pure r-B_4C is expected to form decreases with φ. Also the relative amount of graphite to r-B_4C increases with the φ parameter, which indicates that the formation of graphite is favoured by an increase of the relative amount of carbon content in the reactive atmosphere.

Comparing CVD and LCVD results (Fig. 2) with the thermodynamic equilibrium diagram (Fig. 3), CVD process clearly presents the largest deviation from the equilibrium

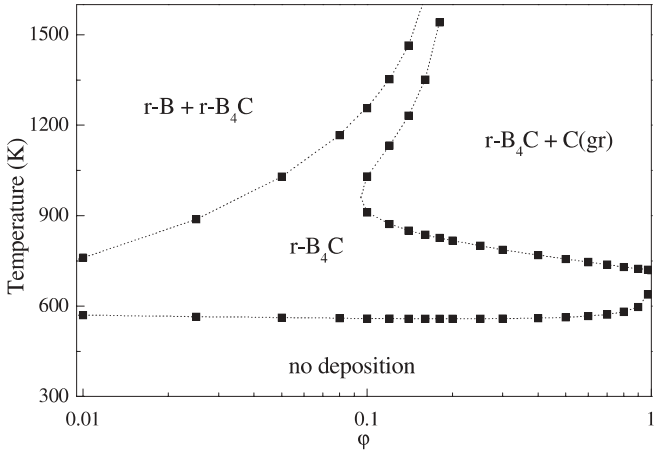

FIGURE 3 Calculated equilibrium distribution of solid phases vs. temperature and gas phase composition, for gas mixtures of BCl_3, CH_4, H_2 and Ar at a total pressure of 1.33×10^4 Pa [40]

diagram. This deviation is mainly due to the existence of a kinetic barrier to carbon deposition from methane which can be related with the low sticking coefficient of this gas [46]. However, irradiation of the gas mixture with a CO_2 laser clearly enhances the methane decomposition rate, bringing the LCVD process closer to equilibrium conditions. Since methane is transparent to the CO_2 laser radiation, the boost decomposition of CH_4 observed in LCVD should be related with the absorption of the radiation by the BCl_3 molecules. Actually, boron trichloride strongly absorbs the infrared radiation, the most intense infrared active mode being the ν_3 asymmetrical stretch vibration at 950.7 cm^{-1} [13]. BCl_3 molecules display an absorption coefficient ranging from 150×10^{-3} cm^{-1} $Torr^{-1}$ to 5×10^{-3} cm^{-1} $Torr^{-1}$ over the frequency range corresponding to the P-branch of CO_2 laser oscillation, with an effective absorption cross section $\sigma = 4.3 \times 10^{-18}$ cm^2 for the P(12) oscillation line, at 951 cm^{-1} [15]. Thus, irradiation of $BCl_3 + CH_4$ mixtures with a CO_2 laser beam leads to heating of the gas phase throughout collisions and vibrational relaxation processes of excited BCl_3 molecules, promoting the observed overcoming of the kinetic barrier to carbon deposition.

This explanation receives further support from the analysis of films processed at atmospheric pressure, for which co-deposition of the two phases, boron carbide and graphite, was observed for φ as low as 0.25 [42]. Figure 4 shows the micro-Raman spectrum of a typical LCVD film grown at atmospheric pressure with $\varphi = 0.25$ and an estimated $T = 1090$ K. The spectrum reveals not only the intra- and inter-icosahedral vibration bands characteristic of r-B_4C but also the "D" and "G" peaks usually assigned to disordered graphite, centred at 1350 and 1578 cm^{-1} respectively. The co-deposition of the two phases is clear evidence that in LCVD deposition takes place much closer to equilibrium, the kinetic barrier to methane decomposition being largely overcome at 1 bar since the increase in total pressure leads to an increase in the net amount of BCl_3 molecules and in their residence time in the chemical reaction zone, which favours the effective heating of the gas phase under laser irradiation.

The possibility of depositing r-B_4C by LCVD at atmospheric pressure is very attractive for industrial applications

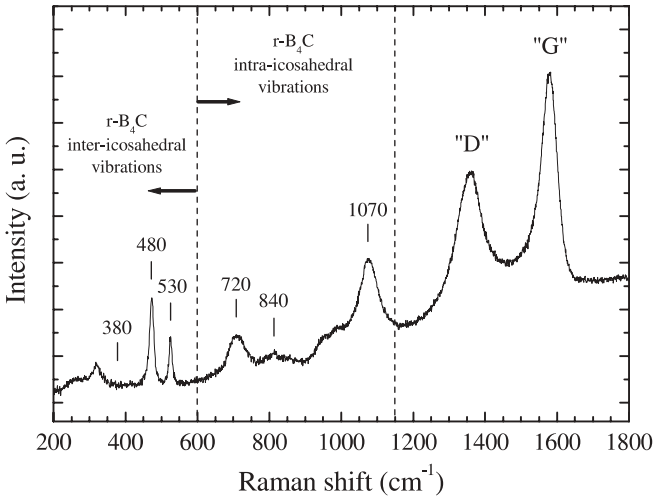

FIGURE 4 Micro-Raman spectrum of a LCVD film produced at atmospheric pressure with $\varphi = 0.25$. The inter- and intra-icosahedral vibrational bands of r-B_4C and the "D" and "G" peaks of graphite are labelled

given the economic aspects and the ease with which the process can be scaled up. Furthermore, by controlling laser power density and the relative amount of carbon and boron precursors in the reactive gas phase, LCVD at atmospheric pressure allows for co-deposition of r-B_4C, an insulating material, and disordered graphite, a semi-metal, which can be beneficial for tailoring the thermal and electronic properties of boron carbide as well as for controlling its mechanical properties.

3.4 CH_4 *versus* C_2H_4*: the role of carbon precursor on the LCVD of* r−B_4C

For the growth of boron carbide films by LCVD based on a CO_2 laser, it is advantageous to replace methane, which has been so far the carbon precursor mostly used in CVD, by ethylene (C_2H_4). In fact, this compound presents a high absorption coefficient of 38.2×10^{-3} cm^{-1} Torr^{-1} [47] at the P(14) spectral line of the CO_2 laser (949.7 cm^{-1}), and a higher sticking coefficient than methane [48].

Following the calculation technique described in [40], the surface temperature achieved at the centre of the films during deposition can be estimated between 800 K and 1100 K for the films grown from methane, and between 780 K and 1430 K for those produced with ethylene. Figure 5 shows the apparent deposition rate of the films deposited from both carbon precursors, as a function of the deposition temperature referred to above. As can be seen herein, the deposition rate is strongly determined by the carbon precursor. For methane, as temperature increases, growth rates slow down and even decrease at the higher temperatures attained due to the development of a depression in the central region of the deposits with increasing temperature (volcano-like effect). The use of ethylene clearly favours the growth of boron carbide, enabling to double the deposition rate values of methane films for temperatures higher than 1000 K. Deposition rates as high as 0.12 μm s^{-1} were measured for C_2H_4, one order of magnitude larger than those obtained in CVD processes with CH_4 [46, 49].

Three combined factors may explain the observed increase in the amount of deposited material when ethylene is used:

i) C_2H_4 has a much higher sticking coefficient [48], thus a higher adsorption probability at the substrate surface which favours surface reactions;
ii) both BCl_3 and C_2H_4 molecules strongly absorb within the wavelength range of the CO_2 laser, thus enhancing the recombination of carbon and boron atoms to form boron carbide;
iii) for each carbon atom resulting from the decomposition of CH_4, four hydrogen atoms are released as products while in the case of C_2H_4 only two hydrogen atoms are produced. The partial pressure of products in the deposition zone is then higher when methane is used, the inhibition of film growth occurs earlier and lower deposition rates are reached.

From the discussion above, it can be concluded that a finer control of the deposition process and film thickness can be achieved in LCVD of boron carbide from ethylene, due to the higher sensitivity of this process regarding the reaction temperature induced by the laser beam.

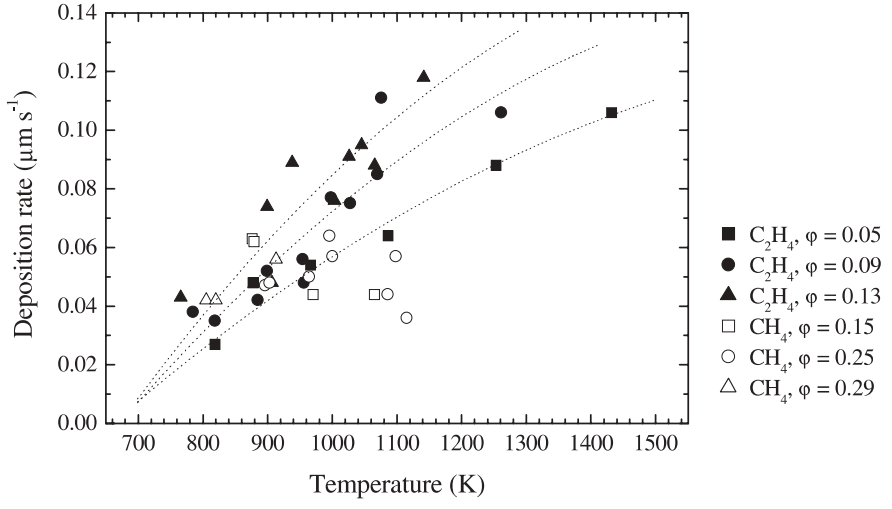

FIGURE 5 Apparent deposition rate of B_4C films prepared at total pressure of 1.33×10^4 Pa from different carbon precursors and carbon containing mixtures vs. estimated surface temperature at the centre of the films

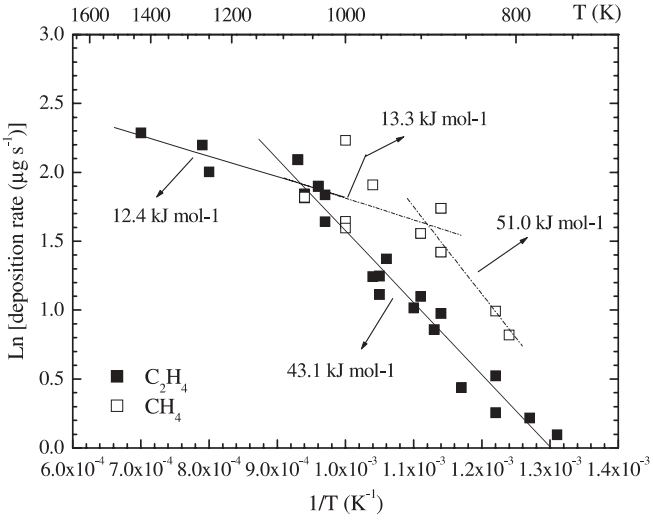

FIGURE 6 Logarithm of the apparent deposition rate as a function of reciprocal temperature. ■, □ measured values; ——, – · – · – least square fitting

Furthermore, one can look at the Arrhenius diagram plotted for the two precursors considered above. This is a common convenient way in CVD to infer on the reaction mechanism that controls deposition. The Arrhenius plot displayed in Fig. 6 shows the logarithm of the r-B_4C apparent deposition rate, calculated in $\mu g\,s^{-1}$ following the method described in [50], as a function of the reciprocal deposition temperature for films grown from $BCl_3 + H_2 + CH_4$ or C_2H_4 gas mixtures. It can be seen that two straight lines with different slopes fit each of the sets of experimental data. Therefore, two rate-limiting mechanisms can be assigned to the deposition process: at high deposition temperature – regime I – film growth is limited by mass transport of the reactive gaseous species, whereas at low deposition temperature – regime II – surface chemical reaction kinetics is the rate-limiting step for film growth.

In regime II, the activation energy is approximately $E_a^{CH_4} = 51.0 \pm 3.9\,kJ\,mol^{-1}$ and $E_a^{C_2H_4} = 43.1 \pm 2.0\,kJ\,mol^{-1}$, while for regime I the difference in slope for both compounds can be neglected within the experimental error. The transition temperature between regimes I and II increases from 894 K for CH_4 to 1071 K for C_2H_4. These features clearly evidence that surface reactions are favoured when C_2H_4 is used as a consequence of a stronger photolytic contribution to the overall deposition process.

It should be also noted that the magnitude of the apparent activation energy deduced for the kinetic regime is much lower than the values that usually characterise this regime in purely thermal CVD processes [51]. In fact, different reaction pathways can be opened between the excited reactants in LCVD leading to a lower activation energy.

4 Laser-assisted deposition of chromium dioxide films

4.1 *Material properties, applications and preparation techniques*

The prospect of building spintronic devices, in which electron spins are used to store and transport information, has attracted considerable attention in recent years [52–54]. Central components of these devices are ferromagnetic materials that provide current with a high degree of spin polarisation. Many of these proposed devices demand carefully controlled growth of ferromagnetic/insulator or ferromagnetic/semiconductor interfaces.

Chromium dioxide (CrO_2) is strongly ferromagnetic at room temperature (Curie temperature, $T_C = 393$ K) and has a half-metallic band structure fully spin-polarised at the Fermi level [55–58], making it extremely attractive for use in those heterostructures. Therefore, much effort has been put into developing efficient and controlled methods for preparing CrO_2 films at sufficiently low temperatures to avoid degradation of the substrate material. Nevertheless, the synthesis of CrO_2 films has been a difficult task due to its metastable nature – CrO_2 is metastable at atmospheric pressure and, if heated, easily decomposes into the insulating antiferromagnetic Cr_2O_3 phase ($T_N = 307$ K) which is the most stable Cr oxide at ambient conditions.

According to the Cr-O phase diagram, chromium dioxide becomes stable under high oxygen pressure (≥ 10 bar) and the higher the temperature, the wider the temperature stability range [59, 60]. Following this pressure dependence, CrO_2 was already prepared via thermal decomposition of CrO_3 and $Cr(OH)_3$, at $T \geq 400\,°C$ and high oxygen pressure of 50–2000 bar, which prevent the transformation of CrO_2 into Cr_2O_3 [61–64]. Alternatively to these high-pressure methods, which are difficult to integrate into multilayer deposition processes, low-pressure deposition techniques (≤ 1 bar) are preferred for the growth of CrO_2 films and layered structures.

Epitaxial thin films of CrO_2 are presently grown on $TiO_2(100)$ and $Al_2O_3(0001)$ by thermal CVD using CrO_3 as chromium precursor [65–70]. CrO_3 is vaporised at 260 °C, carried to the reaction zone by an oxygen flux and thermally decomposed onto a substrate that is heated in the range from 340 to 440 °C. The quality of the layers depends critically on the substrate temperature, the best results being obtained at a substrate temperature of 390 °C. Independent of their thickness, the films exhibit a sharp ferromagnetic transition with a Curie temperature of about 390 K. They also display metallic characteristics, with room temperature resistivity of about 285 μΩ cm, dropping by about two orders of magnitude upon cooling down to 5 K. For a field of 40 kOe, a positive transverse magnetoresistance (MR) of about 25% at 5 K and a negative MR of about 7% at near T_C have been observed.

Besides chromium trioxide, other precursors such as Cr_8O_{21} [71] and CrO_2Cl_2 [72, 73] have also been used for the CVD of CrO_2 layers at temperatures $\sim 400\,°C$, with identical properties to those grown with CrO_3.

Despite thermal CVD achievements, there is a continuous search for deposition methods that allow the growth of CrO_2 thin films at low temperatures. This is indeed of crucial importance to ensure interface quality and the ability to coat thermal-sensitive materials such as those envisaged in spintronic devices.

4.2 *LCVD of* CrO_2 *using UV lasers*

Laser-induced CVD has the potential to meet the requirements stated above. Among the available chromium

chemical precursors, the use of chromium hexacarbonyl – $Cr(CO)_6$ – seems to have some advantages when UV photodeposition of CrO_2 is intended, namely: i) it provides good volatility allowing for easy transport in the gas phase, ii) it strongly absorbs UV radiation in a wide range of wavelengths, and iii) the Cr–CO bond is preferentially broken in the presence of UV radiation.

$Cr(CO)_6$ is a solid with a vapour pressure of ~ 40 Pa at room temperature [74]. Photodissociation of $Cr(CO)_6$ is strongly wavelength dependent; its absorption spectrum consists of several overlapping bands with two intense and broad lines located at 280 nm and 225 nm, assigned to metal-ligand charge transfer states [66, 75]. The energy required to remove one CO ligand is 1.6 eV [76] and complete dissociation to $Cr + 6CO$ requires ~ 10 eV. Nevertheless, this complete dissociation and the additional absorption of photons necessary to produce Cr^+ ions were observed by Mayer et al. [75] at wavelengths as long as 600 nm, by using high laser fluences.

Photolytic decomposition of $Cr(CO)_6$ by UV radiation at $\lambda = 337$ nm (nitrogen laser), carried out in an oxygen environment, led to the growth of thin layers containing CrO_2 [74, 77–79]. The films were deposited onto Si(111) wafers at temperatures between 288 and 304 K [74, 77] and display a behaviour consistent with a two-phase system containing both Cr_2O_3 and CrO_2, the relative amount of each phase depending on the oxygen partial pressure. Figure 7 shows the magnetization as a function of temperature for two films processed with different oxygen partial pressures and 1×10^{-5} Torr of $Cr(CO)_6$. The one deposited at $p_{O_2} = 2 \times 10^{-7}$ Torr exhibits a $T_C = 345 \pm 10$ K. By increasing the O_2 partial pressure to 1×10^{-6} Torr, the amount of CrO_2 increases and the critical temperature becomes 390 ± 10 K, thus approaching the expected Curie temperature.

Of particular interest is the surprising result reported by Perkins et al. [77] that LCVD carried out at low substrate temperature (~ 290 K) favours the growth of high quality CrO_2 films, in contrast with conventional thermal deposition methods. The main reason pointed out for this experimental result is that photodissociation of $Cr(CO)_6$ is a surface controlled process for which dissociation and desorption are competing processes.

Looking for a better efficiency of the photon-molecule interaction leading to $Cr(CO)_6$ photodissociation, it can be advantageous to explore other ultraviolet wavelengths for which $Cr(CO)_6$ the absorption cross section is higher than for the nitrogen laser radiation, as can be seen in Table 2.

A few studies using the KrF excimer laser have been conducted in our group for the same precursors as described above. Instead of static conditions, a continuous flow of the reactants was used, which also allows for easier automation

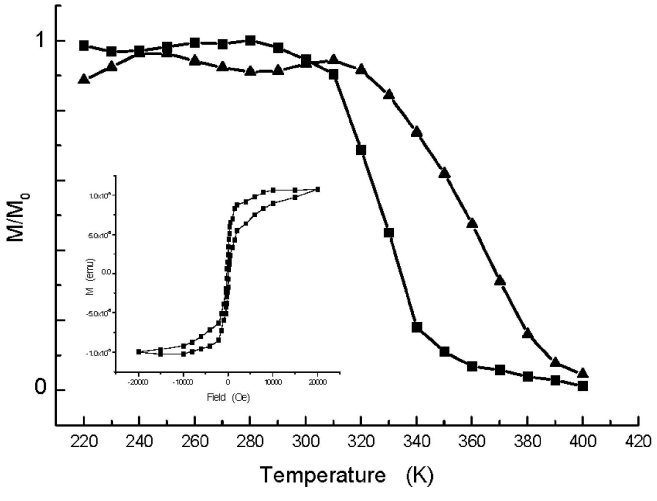

FIGURE 7 Magnetization vs. temperature curves at an applied field of $H = 500$ Oe. ■, film processed at $p_{O_2} = 2 \times 10^{-7}$ Torr; ▲, film processed at $p_{O_2} = 1 \times 10^{-6}$ Torr. The hysteresis loop shown in the *inset* was taken at 100 K for the film produced at $p_{O_2} = 2 \times 10^{-7}$ Torr. Figure adapted from reference [78] with permission

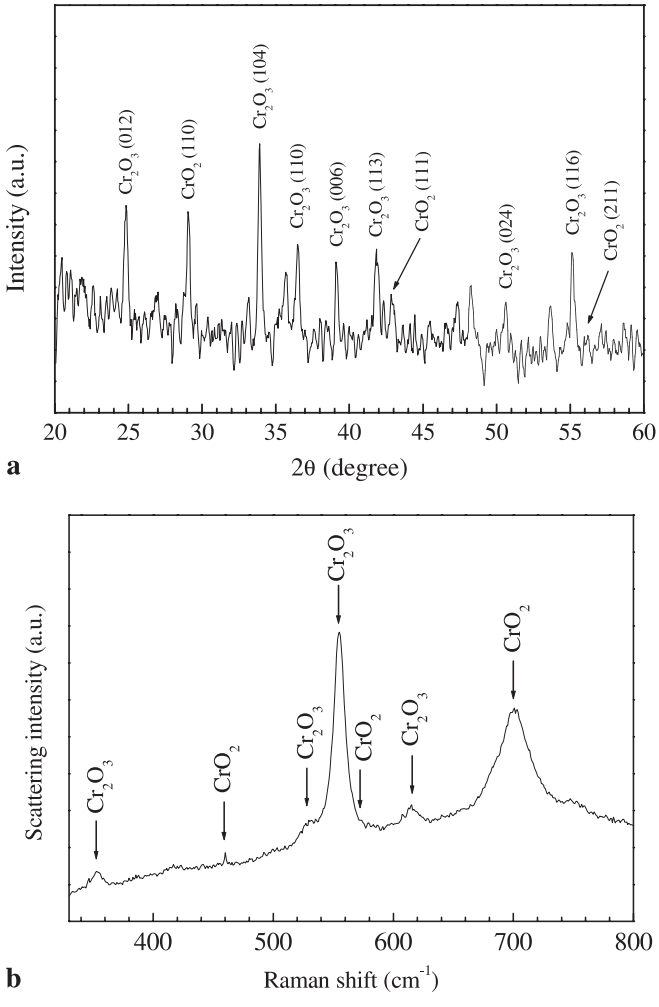

FIGURE 8 XRD pattern (**a**) and micro-Raman spectrum (**b**) of a chromium oxide film deposited using a KrF excimer laser. Experimental parameters: $F = 75$ mJ cm^{-2}, $P_{Total} = 0.5$ mbar, $\Phi_{Cr(CO)_6} = 1$ sccm, $\Phi_{O_2} = 1$ sccm and $\Phi_{Ar} = 50$ sccm

ArF 193 nm	KrF 248 nm	Ar^+ (2ω) 257 nm	XeCl 308 nm	N_2 (337 nm)	Reference
2.6×10^{-17}	5.0×10^{-17}	2.5×10^{-17}	5.5×10^{-18}	$< 10^{-19}$	[66, 80]
	5.3×10^{-17}				[66, 81]
1.2×10^{-17}	3.3×10^{-17}				[66, 82]

TABLE 2 Absorption cross-section (cm^2) of $Cr(CO)_6$ for different UV laser wavelengths

and continuous high-rate coating. The films were grown on $Al_2O_3(0001)$ substrates at room temperature. Figure 8a shows the XRD pattern of a film grown with $p_{Cr(CO)_6} = p_{O_2}$ and a laser fluence of 75 mJ cm^{-2}. Although deposition of a single CrO_2 phase has not been achieved, two significant diffraction peaks clearly match the (110) and (111) planes of CrO_2. The presence of chromium dioxide, co-deposited with chromia, is also evidenced by the broad line at $\sim$700 cm^{-1} (B_{2g} mode) in the micro-Raman spectrum recorded over the same sample (Fig. 8b). A systematic study of the processing parameters has shown that partial pressure ratio $p_{Cr(CO)_6}/p_{O_2}$ and laser fluence are the prominent parameters that have to be carefully controlled in order to increase the content of CrO_2 in the deposited thin films [83].

4.3 *Other possible chemical paths for LCVD of* CrO_2

Despite the stimulating results reported above, the deposition of CrO_2 by LCVD is still an open and challenging research field. Besides the UV laser radiation/$Cr(CO)_6$ combination already discussed, several other laser type/chemical precursor combinations can be profitably explored in order to apply this technique to the growth of CrO_2 films. For instance, Arnone et al. [84] have reported the synthesis of ferromagnetic Cr_2O_3/CrO_2 composite films over a variety of substrates (Si, GaAs, SiO_2 and glass), by visible-laser photodissociation of chromyl chloride (CrO_2Cl_2) using a line-tuneable cw Ar^+ laser (488–515 nm). Another challenging route to achieve CrO_2 synthesis, which to our knowledge has not yet been investigated, would consist of photothermal LCVD based on infrared laser radiation and a chemical precursor with vibrational infrared-active modes. In this experimental approach, the irradiation of oxidizing mixtures containing chromium precursors such as CrO_3, CrO_2Cl_2 or $Cr(C_6H_6)_2$ with a CO_2 laser, can be envisaged since all these compounds have vibrational IR-active modes within the frequency range of the CO_2 laser transitions [85–87].

REFERENCES

1 H.O. Pierson: *Handbook of Chemical Vapor Deposition, Principles, Technology and Applications*, 2nd edition (Noyes Publications, Park Ridge 1999)
2 J.M. Blocher Jr.: In *Deposition Technologies for Films and Coatings*, ed. by R.F. Bunshad (Noyes Publications, Park Ridge 1982)
3 J. Mazumder, A. Kar: *Theoryy and Application of Laser Chemical Vapor Deposition* (Plenum Press, New York 1995)
4 O. Lehmann, M. Stuke: Appl. Phys. A **53**, 343 (1991); O. Lehmann, M. Stuke: Mater. Lett. **21**, 131 (1994)
5 S. Johansson, J.-A. Schweitz, H. Westberg, M. Boman: J. Appl. Phys. **72**, 5956 (1992)
6 F.T. Wallenberger: Science **267**, 1274 (1995)
7 D. Bauerle: *Laser Processing and Chemistry*, 3rd edition (Springer-Verlag, Berlin 2000)
8 Y. Rytz-Froidevaux, R.P. Salathé, H.H. Gilgen: Appl. Phys. A **37**, 121 (1985)
9 R.L. Jackson, T.H. Baum, T.T. Kodas, D.J. Ehrlich, G.W. Tyndall, P.B. Comita: In *Laser Microfabrication: Thin Film Processes and Lithography*, ed. by D.J. Ehrlich, J.Y. Tsao (Academic Press, Boston 1989) p. 385
10 C. Duty, D. Jean, W.J. Lackey: Int. Mater. Rev. **46**, 271 (2001)
11 D.J. Ehrlich, J.Y. Tsao: J. Vac. Sci. Technol. B **1**, 969 (1983)
12 D. Lydtin: In Proc. of the 3rd International Conference on CVD, ed. by F.A. Glaski (Am. Nucl. Soc., Hinsdale 1972) p. 127
13 K. Nakamoto: *Infrared and Raman Spectra of Inorganic and Coordination Compounds*, 5th edition (John Wiley Sons, Inc., New York 1997)
14 J.I. Steinfeld: *Laser and Coherence Spectroscopy* (Plenum Press, New York 1978) pp. 65 and 73
15 N. Karlov: Appl. Opt. **13**, 301 (1974)
16 D. Fernández, P. González, J. Pou, E. García, J. Serra, B. León, M. Perez-Amor, C. Garrido: J. Vac. Sci. Technol. A **12**, 484 (1994)
17 P. González, D. Fernández, J. Pou, E. García, J. Serra, B. León, M. Perez-Amor: Thin Solid Films **218**, 170 (1992)
18 M. Rothschild: In *Laser Microfabrication: Thin Film Processes and Lithography*, ed. by D.J. Ehrlich, J.Y. Tsao (Academic Press, Boston 1989) p. 163
19 S. Veprek: J. Vac. Sci. Technol. A **17**, 2401 (1999)
20 R. Telle: In *Structure and Properties of Ceramics,* Materials Science and Technology, Vol. 11, ed. by M.V. Swain (VCH Publishers, Weinheim 1994) p. 173
21 D. Emin: Phys. Rev. B **38**, 6041 (1988)
22 M. Olsson, S. Soderberg, B. Stridh, U. Jansson, J.-O. Carlsson: Thin Solid Films **172**, 95 (1989)
23 T.L. Aselage, D. Emin, S.S. McCready, R.V. Duncan: Phys. Rev. Lett. **81**, 2316 (1998)
24 X. Deschanels, D. Simeone, J.P. Bonal: J. Nucl. Mater. **265**, 321 (1999)
25 F. Mauri, N. Vast, C.J. Pickard: Phys. Rev. Lett. **87**, 85 506 (2001)
26 I. Jiménez, D.G.J. Sutherland, T. van Buuren, J.A. Carlisle, L.J. Terminello, F.J. Himpsel: Phys. Rev. B **57**, 13 167 (1998)
27 R. Talant, T.L. Aselage, A.N. Campbell, D. Emin: Phys. Rev. B **40**, 5649 (1989)
28 T.L. Aselage, D.R. Tallant, J.H. Gieske: In *The Physics and Chemistry of Carbides, Nitrides and Borides*, ed. by R. Freer (Kluwer Academic Publishers 1990) p. 97
29 R. Lazzari, N. Vast, J.M. Besson, S. Baroni, A. Dal Corso: Phys. Rev. Lett. **16**, 3230 (1999)
30 U. Jansson, J.-O. Carlsson, B. Stridh, S. Soderberg, M. Olsson: Thin Solid Films **172**, 81 (1989)
31 M. Olsson, S. Soderberg, B. Stridh, U. Jansson, J.-O. Carlsson: Thin Solid Films **172**, 95 (1989)
32 U. Jansson, J.-O. Carlsson, L.C. Markert, J.E. Green: J. Vac. Sci. Technol. A **7**, 3172 (1989)
33 U. Jansson, J.-O. Carlsson: J. Vac. Sci. Technol. A **6**, 1733 (1988)
34 J. Rey, G. Male, Ph. Kapsa, J.L. Loubet: J. Physique, Coll. C5 **50**, 311 (1989)
35 D.N. Kevill, T.J. Rissmann, D. Brewe, C. Wood: J. Crystal Growth **74**, 210 (1986)
36 C.I. Chiang, H. Holleck, O. Meyer: Nucl. Instrum. Methods Phys. Res. B **91**, 692 (1994)
37 M.A. McKernan: Surf. Coatings Technol. **49**, 411 (1991)
38 P.D. Kervalishvili, S.O. Shalamberidze, Y.A. Bokowsky: AIP Conf. Proc. **231**, 524 (1991)
39 J.C. Oliveira, M.N. Oliveira, O. Conde: Surf. Coatings Technol. **80**, 100 (1996)
40 J.C. Oliveira, O. Conde: Thin Solid Films **307**, 295 (1997)
41 O. Conde, A.J. Silvestre, J.C. Oliveira: Surf. Coatings Technol. **125**, 141 (2000)
42 J.C. Oliveira, P. Paiva, M.N. Oliveira, O. Conde: Appl. Surf. Sci. **138–139**, 159 (1999)
43 M.J. Santos, A.J. Silvestre, O. Conde: Surf. Coatings Technol. **151**, 160 (2002)
44 A.J. Silvestre, M.J. Santos, O. Conde: Key Eng. Mater. **230–232**, 56 (2002)
45 G. Eriksson: Acta Chem. Scand. **25**, 2651 (1971)
46 U. Jansson, J.-O. Carlsson, B. Stridh: J. Vac. Sci. Technol. A **5**, 2823 (1987)
47 R.R. Patty, G.M. Russwurm, W.A. McClenny, D.R. Morgan: Appl. Opt. **13**, 2850 (1974)
48 M. Boman, J.-O. Carlsson: Surf. Coatings Technol. **49**, 221 (1991)
49 O. Postel, J. Heberlein: Surf. Coatings Technol. **108–109**, 247 (1998)
50 M.L.F. Paramês, O. Conde: Appl. Surf. Sci. **109–110**, 554 (1997)
51 J.-O. Carlsson: In *Advanced Surface Coatings – A Handbook of Surface Engineering*, ed. by D.S. Rickerby, A. Matthews (Chapman & Hall, New York 1991), p. 162
52 G.A. Prinz: Phys. Today **48**, 58 (1995)
53 D. Grundler: G.A. Prinz: Science **282**, 1660 (1998)
54 D. Grundler: Phys. World **15**, 39 (2002)
55 K.J. Schwartz: J. Phys. F: Methods Phys. **16**, L211 (1986)
56 M.A. Korotin, V.I. Anisimov, D.I. Khomskii, G.A. Sawatzky: Phys. Rev. Lett. **80**, 4305 (1998)

57 R.J. Soulen, Jr., J.M. Byers, M.S. Osofsky, B. Nadgorny, T. Ambrose, S.F. Cheng, P.R. Broussard, C.T. Tanaka, J. Nowak, J.S. Moodera, A. Barry, J.M.D. Coey: Science **282**, 85 (1998)
58 Y. Ji, G.J. Strijkers, F.Y. Yang, C.L. Chien, JM. Byers, A. Anguelouch, G. Xiao, A. Gupta: Phys. Rev. Lett. **86**, 5585 (2001)
59 B. Kubota: J. Am. Ceram. Soc. **44**, 239 (1961)
60 R.C. De Vries: Mater. Res. Bull. **1**, 83 (1966)
61 T.J. Swoboda, P. Arthur, Jr., N.L. Cox, J.N. Ingraham, A.L. Oppgard, M.S. Sadler: J. Appl. Phys. **32**, 374S (1961)
62 Y. Shibasaki: Mater. Res. Bull. **5**, 1051 (1970)
63 L. Ben-Dor: J. Cryst. Growth **24**, 175 (1974)
64 L. Ranno A. Barry, J.M.D. Coey: J. Appl. Phys. **81**, 5774 (1997)
65 K. Suzuki, P.M. Tedraw: Phys. Rev. B **58**, 11 597 (1998)
66 K. Suzuki, P.M. Tedraw: Appl. Phys. Lett. **74**, 428 (1999)
67 X.W. Li, A. Gupta, T.R. McGuire, P.R. Duncombe, G. Xiao: J. Appl. Phys. **85**, 5585 (1999)
68 X.W. Li, A. Gupta, G. Xiao: Appl. Phys. Lett. **75**, 713 (1999)
69 A. Gupta, X.W. Li, S. Guha, G. Xiao: Appl. Phys. Lett. **75**, 2996 (1999)
70 M. Rabe, J. Pommer, K. Samm, B. Özyilmaz, C. König, M. Fraune, U. Rüdiger, G. Güntherodt, S. Senz, D. Hess: J. Phys.: Condens. Matter **4**, 7 (2002)
71 P.G. Ivanov, S.M. Watts, D.M. Lind: J. Appl. Phys. **89**, 1035 (2001)
72 W.J. DeSisto, P.R. Broussard, T.F. Ambrose, B.E. Nadgorny, M.S. Osofsky: Appl. Phys. Lett. **76**, 3789 (2000)
73 A. Anguelouch, A. Goupta, G. Xiao, D.W. Abraham, Y. Ji, S. Ingvarsson, C.L. Chien: Phys. Rev. B **64**, 180408(R) (2001)
74 P.A. Dowben, Y.G. Kim, S. Baral-Tosh, G.O. Ramseyer, C. Hwang, M. Onellion: J. Appl. Phys **67**, 5658 (1990)
75 T.M. Mayer, G.J. Fisanik, T.S. Eichelberger: J. Appl. Phys. **53**, 8462 (1982)
76 K.E. Lewis, D.M. Golden, G.P. Smith: J. Am. Chem. Soc. **106**, 3905 (1984)
77 F.K. Perkins, C. Hwang, M. Onllion, Y.-G. Kim, P.A. Dowben: Thin Solid Films **198**, 317 (1991)
78 R. Cheng, C.N. Borca, P.A. Dowbwn: Mater. Res. Soc. Symp. Proc. **614**, F10.4.1 (2000)
79 R. Cheng, C.N. Borca, P.A. Dowben, S. Stadler, Y.U. Idzerda: Appl. Phys. Lett. **78**, 521 (2001)
80 T.M. Mayer, G.J. Fisanik, T.S. Eichelberger: J. Appl. Phys. **53**, 8462 (1982)
81 W. Tumas, B. Gilin, A.M. Rosan, J.T. Yardley: J. Am. Chem. Soc. **104**, 55 (1982)
82 D.K. Flynn, J.I. Steinfeld, D.S. Sethi: J. Appl. Phys. **59**, 3914 (1982)
83 P.M. Sousa: Ph.D. Thesis, University of Lisbon (work in progress)
84 C. Arnone, M. Rothschild, J.G. Black, D.J. Ehrlich: Appl. Phys. Lett. **48**, 1018 (1986)
85 M. Zhou, L. Andrews: J. Chem. Phys. **111**, 4230 (1999)
86 G.V. Chertihin, W.D. Bare, L. Andrews: J. Chem. Phys. **107**, 2798 (1997)
87 K. Nakamoto: In *Infrared, Raman spectra of inorganic, coordination compounds*, 5th edition (John Wiley & Sons, New York 1997)